Nationaal Lucht- en Ruimtevaartlaboratorium

National Aerospace Laboratory NLR

Executive summary

Beamforming on moving sources

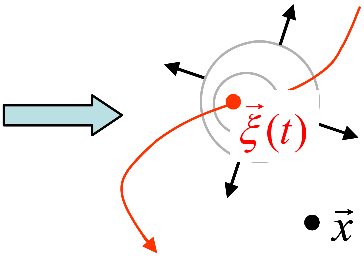

Description of work
In this paper, the theory is described of phased array beamforming on moving sources, in the presence of wind. Applications are discussed for wind turbine and aircraft fly-over measurements.

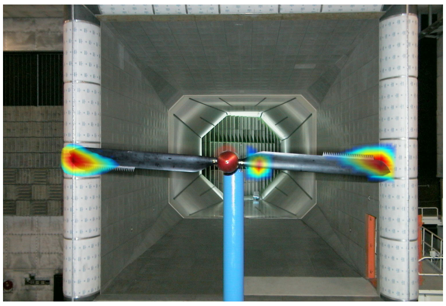

Results and conclusions
In most applications of phased microphone arrays, source location is done on stationary objects like wind tunnel models. However, microphone arrays also offer the opportunity to locate sources on moving objects, even when the motion is not in a straight line. In this paper, a source location technique is described that is applicable to objects in any subsonic motion. The presence of a uniform flow is included in this technique, thus enabling source location measurements on arbitrarily moving objects in wind tunnels. After some modification, the technique can even be applied to out-of-flow array measurements in open wind tunnel configurations. Successful applications of this technique are discussed in the case of a rotating motion (rotating whistles, helicopter rotor, wind turbine), and of a steady, linear motion (fly-over measurements at Schiphol Airport).

Applicability
The technique described in this paper can be applied to sources in any subsonic motion.

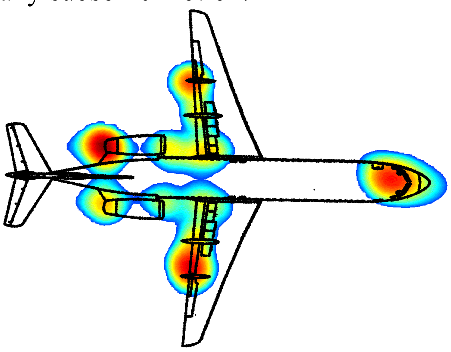

.

Report no.
NLR-TP-2006-733

Author(s)
P. Sijtsma

Report classification
Unclassified

Date
May 2007

Knowledge area(s)
Aëro-akoestisch en experimenteel aërodynamisch onderzoek

Descriptor(s)
Microphone arrays
Wind tunnels
Wind turbines
Moving sources
Fly-Over measurements

This paper was presented as part of the VKI/EWA Lecture Series on “Experimental Aeroacoustics”, Brussels, 13-17 November 2006.

Nationaal Lucht- en Ruimtevaartlaboratorium, National Aerospace Laboratory NLR

Anthony Fokkerweg 2, 1059 CM Amsterdam,
P.O. Box 90502, 1006 BM Amsterdam, The Netherlands
Telephone +31 20 511 31 13, Fax +31 20 511 32 10, Web site: www.nlr.nl

Nationaal Lucht- en Ruimtevaartlaboratorium
National Aerospace Laboratory NLR

NLR-TP-2006-733

Beamforming on moving sources

P. Sijtsma

This paper was presented as part of the VKI/EWA Lecture Series on "Experimental Aeroacoustics", Brussels, 13-17 November 2006.

This publication has been refereed by the Advisory Committee AEROSPACE VEHICLES.

Customer	European Commission
Contract number	ANE3-CT-2004-502889
Owner	NLR + partner(s)
Division	Aerospace Vehicles
Distribution	Unlimited
Classification of title	Unclassified
	May 2007

Approved by:

Author	Reviewer	Managing department
PS 23/1/07	SO 29/1/07	23/1

Summary

In this paper, the theory is described of phased array beamforming on moving sources, in the presence of wind. The theory was implemented for rotating sources, and for sources in steady, linear motion. Successful applications of the theory are discussed for rotating whistles, a helicopter rotor, a wind turbine model, and aircraft fly-over measurements at Schiphol Airport.

Contents

1	**Introduction**	**7**
2	**Theory**	**8**
2.1	Source description	8
2.1.1	Uniform flow	8
2.1.2	Effects of wind tunnel shear layer	10
2.2	Reconstruction of source signals	11
2.3	Reconstruction of source auto-powers	13
2.3.1	Straightforward method	13
2.3.2	Error estimate	13
2.3.3	Alternative method	13
3	**Applications to rotating sources**	**14**
3.1	Computer program ROSI	14
3.2	Rotating whistles	14
3.3	Helicopter blades	16
3.4	Wind turbine blades	17
4	**Fly-over measurements**	**20**
4.1	Test campaign at Schiphol Airport	20
4.2	Aircraft tracking	21
4.3	Array design	22
4.4	Typical results	24
References		**26**

Abbreviations

Symbols

A	source power
$\tilde{A}$	source power estimate
a	complex pressure amplitude at source
c	speed of sound
F	transfer function from moving source to receiver
F_n	transfer function from moving source to n-th microphone
f	frequency
G	Green's function
k	sample index
$\vec{M}$	Mach number vector, Eq. (21)
m	microphone index
N	number of microphones
n	microphone index
R	effective array radius
t	time
t_n	reception time at n-th microphone
$\vec{U}$	uniform flow speed
$\vec{U}_{\mathrm{cor}}$	flow speed corrected for out-of-flow measurements
$\vec{x}_n$	position of n-th microphone

Greek

β	see Eq. (21)
γ	auxiliary function in Eq. (11)
Δt_e	emission time delay
δ	Dirac delta function
$\varepsilon_n(t)$	noise on n-th microphone
$\chi(\vec{x},t)$	acoustic pressure
$\chi_n(t)$	acoustic pressure measured by n-th microphone
$\chi_{n,k}$	sampled acoustic pressure measured by n-th microphone
$\sigma(t)$	emitted source signal
$\tilde{\sigma}(t)$	estimated source signal
$\vec{\zeta}_s(\tau_e)$	intersection of acoustic ray and shear layer
τ	integration parameter (time)
τ_e	emission time
τ_0	zero of auxiliary function γ, Eq. (11)
$\vec{\xi}$	source position

Superscript

$(\cdot)^*$	complex conjugate

Subscript

$(\cdot)_1$	transformed according to Eq. (5)
$(\cdot)_k$	for k-th sample
$(\cdot)_m$	for m-th microphone
$(\cdot)_n$	for n-th microphone

Operator

∇	Nabla operator: $\nabla = (\partial/\partial x, \partial/\partial y, \partial/\partial z)$

Abbreviations

AC	Alternating Current
CB	Conventional Beamforming
CSM	Cross-Spectral Matrix
DNW	German-Dutch Wind Tunnels
FFT	Fast Fourier Transform
LLF	Large Low-speed Facility
MOSI	MOving Source Identifier
ROSI	ROtating Source Identifier

1 Introduction

In most applications of phased microphone arrays, source location is done on stationary objects like wind tunnel models. However, microphone arrays also offer the opportunity to locate sources on moving objects. The first applications to moving sources were reported on trains passing by (Refs. 1, 2), and on airplanes flying over (Refs. 3, 4). Source signals in the moving frame were recalculated from the microphone signals, using the technique of de-Dopplerization (Refs. 5, 6).

The above mentioned examples of array measurements apply to objects moving at constant speed in a straight line. There is, however, no need for a restriction to such a motion. In this lecture, a source location technique is described that is applicable to objects in any subsonic motion. The presence of a uniform flow will be included in this technique, thus enabling source location measurements on arbitrarily moving objects in wind tunnels. After some modification, the technique can even be applied to out-of-flow array measurements in open wind tunnel configurations.

The array technique for moving sources was designed for application to a special type of motion: rotation (Ref. 7). A computer program, named ROSI ("ROtating Source Identifier"), was written to locate rotating sources in a uniform flow. The motivation to develop ROSI was to have the ability to locate and estimate trailing edge noise sources on blades of a wind turbine model in the open jet of the DNW-LLF using an out-of-flow acoustic array (Ref. 8).

This application, which turned out to be successful, was preceded by two other experiments. First, a test was conducted with rotating whistles, producing tonal noise, in the anechoic chamber of the NLR Small Anechoic Wind Tunnel KAT. This set-up was designed specifically to test the software. Secondly, measurements were carried out on helicopter blades in the open jet of the DNW-LLF.

In this lecture, the theory behind ROSI is described and typical results of the three experiments are given. Parallel to these rotating source applications, the technique was also applied to aircraft fly-over measurements at Amsterdam Airport Schiphol (Refs. 9, 10). After a few modifications, the ROSI software was renamed into MOSI ("MOving Source Identifier"). In this lecture, a brief description of these fly-over measurements is given too.

2 Theory

For array measurements on moving objects, the correct acoustic transfer function from moving source to receiver is required, incorporating the effect of Doppler frequency shift. For that purpose, an expression will be used for a moving monopole source in a uniform flow. A brief derivation of such an expression is given below. For a more thorough approach, the reader is referred to Ref. 11. Using this transfer function, and by proper interpolation of the sampled microphone data, the signals emitted by the moving sources can be reconstructed. This beamforming technique is necessarily carried out in the time-domain. It will be explained, however, that the signal/noise ratio can be enlarged by a technique, which is similar to the frequency-domain technique of removing the main diagonal from the cross-spectral matrix (CSM).

2.1 Source description

2.1.1 Uniform flow

The acoustic pressure field χ of a monopole source moving in a uniform flow is governed by the differential equation:

$$\nabla^2 \chi - \frac{1}{c^2}\left(\frac{\partial}{\partial t} + \vec{U}\cdot\nabla\right)^2 \chi = \sigma(t)\delta\left(\vec{x} - \vec{\xi}(t)\right), \tag{1}$$

in which $\vec{\xi}(t)$ is the time-dependent source position. Following Dowling and Ffowcs Williams (Ref. 12), (1) can be solved by writing the right-hand side as a superposition:

$$\nabla^2 \chi - \frac{1}{c^2}\left(\frac{\partial}{\partial t} + \vec{U}\cdot\nabla\right)^2 \chi = \int_{-\infty}^{\infty} \sigma(\tau)\delta\left(\vec{x} - \vec{\xi}(\tau)\right)\delta(t-\tau)d\tau\,. \tag{2}$$

Then, the solution can be expressed as

$$\chi(\vec{x},t) = \int_{-\infty}^{\infty} \sigma(\tau)G\left(\vec{x},\vec{\xi}(\tau),t,\tau\right)d\tau\,, \tag{3}$$

where G (the "Green's function") is a solution of

$$\nabla^2 G - \frac{1}{c^2}\left(\frac{\partial}{\partial t} + \vec{U}\cdot\nabla\right)^2 G = \delta\left(\vec{x} - \vec{\xi}(\tau)\right)\delta(t-\tau)\,. \tag{4}$$

The solution of (4) can be derived from the Green's function of the ordinary wave equation (Ref. 13) by using the following co-ordinate transformation:

$$\begin{cases} t_1 = t, \\ \vec{x}_1 = \vec{x} - \vec{U}t. \end{cases} \tag{5}$$

In the transformed system, we have:

$$\nabla_1^{\,2} G - \frac{1}{c^2}\frac{\partial^2 G}{\partial t_1^{\,2}} = \delta\left(\vec{x}_1 + \vec{U}t_1 - \vec{\xi}(\tau)\right)\delta(t_1 - \tau) = \delta\left(\vec{x}_1 + \vec{U}\tau - \vec{\xi}(\tau)\right)\delta(t_1 - \tau). \tag{6}$$

The causal solution of (6) is:

$$G = -\frac{\delta\left(t_1 - \tau - \frac{1}{c}\left\|\vec{x}_1 + \vec{U}\tau - \vec{\xi}(\tau)\right\|\right)}{4\pi\left\|\vec{x}_1 + \vec{U}\tau - \vec{\xi}(\tau)\right\|}. \tag{7}$$

Therefore, the causal solution of (4), in other words the pressure field induced by an impulsive blow in a uniform flow, is

$$G\left(\vec{x}, \vec{\xi}(\tau), t, \tau\right) = -\frac{\delta\left(t - \tau - \frac{1}{c}\left\|\vec{x} - \vec{\xi}(\tau) - \vec{U}(t-\tau)\right\|\right)}{4\pi\left\|\vec{x} - \vec{\xi}(\tau) - \vec{U}(t-\tau)\right\|}, \tag{8}$$

in which $t > \tau$. It follows that the solution of (2), and hence the solution of (1) is

$$\chi(\vec{x}, t) = -\int_{-\infty}^{\infty} \frac{\sigma(\tau)\delta\left(t - \tau - \frac{1}{c}\left\|\vec{x} - \vec{\xi}(\tau) - \vec{U}(t-\tau)\right\|\right)}{4\pi\left\|\vec{x} - \vec{\xi}(\tau) - \vec{U}(t-\tau)\right\|}\, d\tau. \tag{9}$$

To elaborate this integral, introduce the emission time $\tau_e(t)$ as the solution of

$$t - \tau_e = \frac{1}{c}\left\|\vec{x} - \vec{\xi}(\tau_e) - \vec{U}(t - \tau_e)\right\|. \tag{10}$$

As long as the motion is subsonic, this solution is unique. Using (10) and the identity (Ref. 12)

$$\int_{-\infty}^{\infty} f(\tau)\delta\big(\gamma(\tau)\big)\,d\tau = \sum \frac{f(\tau_0)}{|\gamma'(\tau_0)|},\ \text{where } \gamma(\tau_0) = 0\,, \tag{11}$$

Eq. (9) can be worked out as

$$\chi(\vec{x},t) = \frac{-\sigma(\tau_e)}{4\pi\left\{c\big(t-\tau_e\big) + \frac{1}{c}\Big(-\vec{\xi}'(\tau_e) + \vec{U}\Big)\cdot\Big(\vec{x} - \vec{\xi}(\tau_e) - \vec{U}(t-\tau_e)\Big)\right\}}\,. \tag{12}$$

The denominator of (12) includes the "convective amplification", that is experienced when the source moves towards the observer. The perceived, Doppler-shifted frequency can be derived from (10), by multiplying the emitted frequency with $\partial\tau_e/\partial t$.

The transfer function *F* from moving source in $\vec{\xi}(t)$ to receiver in $\vec{x}$ is given by

$$F\Big(\vec{x},\vec{\xi}(\tau_e),t,\tau_e\Big) = \frac{\chi(\vec{x},t)}{\sigma(\tau_e)} = \frac{-1}{4\pi\left\{c\big(t-\tau_e\big) + \frac{1}{c}\Big(-\vec{\xi}'(\tau_e) + \vec{U}\Big)\cdot\Big(\vec{x} - \vec{\xi}(\tau_e) - \vec{U}(t-\tau_e)\Big)\right\}}\,, \tag{13}$$

where the relation between t and τ_e is given by (10).

It is noted that, in general, an explicit solution for τ_e as a function of t does not exist. For source reconstruction, this is not a limitation, because we can solve the inverse problem, i.e., derive from (10) an expression for t as a function of τ_e. This is worked out in Section 2.2.

2.1.2 Effects of wind tunnel shear layer

The transfer function *F*, derived in the foregoing section, is valid for sources in a uniform flow. In other words, the receiver $\vec{x}$ has to be in the same flow as the source $\vec{\xi}$. Hence, it is not valid for out-of-flow array measurements in an open jet wind tunnel.

However, the effect of transmission through the shear layer can be easily incorporated in the transfer function by replacing in (10) and (13) the uniform flow $\vec{U}$ by the average flow $\vec{U}_{\text{cor}}$ between source and receiver. For instance, if the acoustic ray from source to receiver cuts through the shear layer in $\vec{\zeta}_s(\tau_e)$, then the corrected flow is given by

$$\vec{U}_{\mathrm{cor}} = \vec{U} \frac{\left\| \vec{\zeta}(\tau_e) - \vec{\xi}(\tau_e) \right\|}{\left\| \vec{x} - \vec{\xi}(\tau_e) \right\|}. \tag{14}$$

This shear layer correction, which may seem a little crude, has been extensively compared with two more sophisticated methods: the Amiet correction (Ref. 14) for an infinitely thin shear layer, and "ray acoustics" (Ref. 15) incorporating the finite thickness of the shear layer. This comparison was done through microphone array simulations with a non-moving monopole source. It revealed that the differences in array output between the three methods were negligible, as long as the flow speed is moderate (say $\left\|\vec{U}\right\| \le 85$ m/s) and the angles between the shear layer and the acoustic rays are not too small (say $\ge 45°$).

2.2 Reconstruction of source signals

Suppose $\chi_n(t),\ n = 1,...,N$ are the acoustic pressures, recorded by the *N* microphones. If a monopole source with time-dependent position $\vec{\xi}(t)$ is present, then we can write for the microphone signals

$$\chi_n(t) = F\left(\vec{x}_n, \vec{\xi}(\tau_e), t, \tau_e\right)\sigma(\tau_e) + \varepsilon_n(t), \tag{15}$$

where $\varepsilon_n(t)$ is noise and/or contributions from other sources.

In order to reconstruct the source signal $\sigma(\tau)$ from the microphone signals $\chi_n(t)$, we take in (15) a fixed emission time τ_e, independent of microphone number. Then the receiver time *t* depends on *n*, as follows from (10):

$$t_n - \tau_e = \frac{1}{c}\left\| \vec{x}_n - \vec{\xi}(\tau_e) - \vec{U}(t_n - \tau_e) \right\|. \tag{16}$$

Hence, (15) is written as

$$\chi_n(t_n) = F\left(\vec{x}_n, \vec{\xi}(\tau_e), t_n, \tau_e\right)\sigma(\tau_e) + \varepsilon_n(t_n), \tag{17}$$

which is abbreviated to

$$\chi_n(t_n) = F_n(t_n, \tau_e)\sigma(\tau_e) + \varepsilon_n(t_n). \tag{18}$$

The solution of (16) for t_n as function of τ_e is:

$$t_n = \tau_e + \Delta t_e \,, \tag{19}$$

with

$$\Delta t_e = \frac{1}{c\beta^2}\left(-\vec{M}\cdot\left(\vec{x}_n - \vec{\xi}(\tau_e)\right) + \sqrt{\left\{\vec{M}\cdot\left(\vec{x}_n - \vec{\xi}(\tau_e)\right)\right\}^2 + \beta^2 \left\|\vec{x}_n - \vec{\xi}(\tau_e)\right\|^2}\right), \tag{20}$$

in which

$$\vec{M} = \vec{U}/c \text{ and } \beta^2 = 1 - \left\|\vec{M}\right\|^2 . \tag{21}$$

A reconstructed source signal $\tilde{\sigma}(\tau_e)$ can be found with the delay-and-sum procedure:

$$\tilde{\sigma}(\tau_e) = \frac{1}{N}\sum_{n=1}^{N} \tilde{\sigma}_n(\tau_e) \,, \tag{22}$$

with

$$\tilde{\sigma}_n(\tau_e) = \chi_n(t_n)/F_n(t_n,\tau_e) \,. \tag{23}$$

If the acoustic pressures are like (18), then we have:

$$\tilde{\sigma}(\tau_e) = \sigma(\tau_e) + \frac{1}{N}\sum_{n=1}^{N} \varepsilon_n(t_n)/F_n(t_n,\tau_e) \,. \tag{24}$$

It is noted that t_n, as calculated by (19), does not need to coincide with a sample time $k\Delta t$. The best way to deal with this is to linearly interpolate the sampled data:

$$\chi_n(t_n) \approx \chi_{n,k}\left((k+1) - \frac{t_n}{\Delta t}\right) + \chi_{n,k+1}\left(\frac{t_n}{\Delta t} - k\right). \tag{25}$$

To avoid the frequency spectrum from being spoiled by aliasing from higher frequencies, the sample frequency should be taken significantly higher than two times the maximum analysis frequency, but the cut-off frequency for the anti-aliasing filter should be relatively low. This issue is considered in Ref. 6.

2.3 Reconstruction of source auto-powers

2.3.1 Straightforward method

A straightforward way to calculate the frequency spectrum of a source signal is to evaluate (22) for $\tau_e = k\Delta t,\ k = 1,...,K$ and then perform an FFT, resulting in complex pressure amplitudes:

$$a(\tilde{\sigma}) = \frac{1}{N}\sum_{n=1}^{N} a(\tilde{\sigma}_n)\,. \tag{26}$$

The source auto-power estimate $\tilde{A}$ is calculated as:

$$\tilde{A} = \frac{1}{2}\left|a(\tilde{\sigma})\right|^2 = \frac{1}{2N^2}\left|\sum_{n=1}^{N} a(\tilde{\sigma}_n)\right|^2 = \frac{1}{2N^2}\sum_{m=1}^{N}\sum_{n=1}^{N} a(\tilde{\sigma}_m)a(\tilde{\sigma}_n)^*\,. \tag{27}$$

2.3.2 Error estimate

With (24) and (27), we can write

$$\tilde{A} = \frac{1}{2}\left|a(\sigma) + \frac{1}{N}\sum_{n=1}^{N} a\left(\varepsilon_n / F_n\right)\right|^2. \tag{28}$$

Now assume that $\varepsilon_n(t)$ is stochastic and incoherent from one microphone to the other (e.g. wind noise). Then, after averaging, the following expression remains:

$$\tilde{A} = \frac{1}{2}\left|a(\sigma)\right|^2 + \frac{1}{2N^2}\sum_{n=1}^{N}\left|a\left(\varepsilon_n / F_n\right)\right|^2 = A + \frac{1}{2N^2}\sum_{n=1}^{N}\left|a\left(\varepsilon_n / F_n\right)\right|^2\,. \tag{29}$$

2.3.3 Alternative method

Consider the following approximation of (27):

$$\tilde{A} = \frac{1}{2N(N-1)}\sum_{m=1}^{N}\sum_{\substack{n=1\\ n\neq m}}^{N} a(\tilde{\sigma}_m)a(\tilde{\sigma}_n)^* = \frac{1}{2N(N-1)}\left(\left|\sum_{n=1}^{N} a(\tilde{\sigma}_n)\right|^2 - \sum_{n=1}^{N}\left|a(\tilde{\sigma}_n)\right|^2\right). \tag{30}$$

Again under the assumption that $\varepsilon_n(t)$ is stochastic and incoherent, and after averaging over many time periods, we simply get $\tilde{A} = A$. In other words, the expected error is zero now.

This alternative method is analogous to the elimination of the main diagonal from the CSM. Just like its frequency-domain counterpart, the right-hand side of (30) may become negative, which is not physical.

3 Applications to rotating sources

3.1 Computer program ROSI

Based on the theory described in the previous chapter, the computer program ROSI was written to locate rotating sources and to reconstruct their emitted signals. ROSI assumes point sources with unidirectional directivity (monopoles). However, any other a priori known directivity could be included by converting the right-hand side of (1) into a multipole expansion. The rotational speed is determined by pulses which are generated once per revolution. This chapter presents a number of ROSI applications. It is a summary of the results presented in Ref. 7.

3.2 Rotating whistles

For validation of ROSI, an experiment in the anechoic chamber of the NLR Small Anechoic Wind Tunnel KAT was set up, consisting of microphone array measurements on rotating sources. The rotating sources were two whistles producing pure tones at different frequencies. The whistles were mounted at the tips of two tubes connected to an exciter (Fig. 1). The radius of the circle described by the whistles was 0.56 m. The array used in this experiment consisted of 35 microphones arranged in a sparse 2D set-up. In order to record Doppler-shifted frequencies, the array was positioned at an oblique view angle. Both the frequency of the whistles and the rotational speed of the tubes were varied in the experiment. Here, we consider the frequencies 3150 Hz (whistle 1) and 5000 Hz (whistle 2), and 354 RPM for the rotational speed.

When the whistles are rotating, the measured frequencies are Doppler-shifted. This is illustrated in Fig. 2, where the average microphone spectra are compared for non-rotating and rotating whistles. Nevertheless, as shown in the source maps of Fig. 3, ROSI is able to locate the positions of the whistles. The source maps of Fig. 3 show the results of averaging over several revolutions. The source locations shown in the maps correspond to a reference geometry, viz. the positions at the time of the pulse (see Section 3.1).

The ability of ROSI to determine the source levels of the rotating whistles is shown in Fig. 4, where the average microphone spectrum for non-rotating whistles is compared with spectra reconstructed by ROSI in case of rotating whistles. In general, the ROSI results are good. For 5000 Hz, there is a small reduction in peak frequency due to directivity effects.

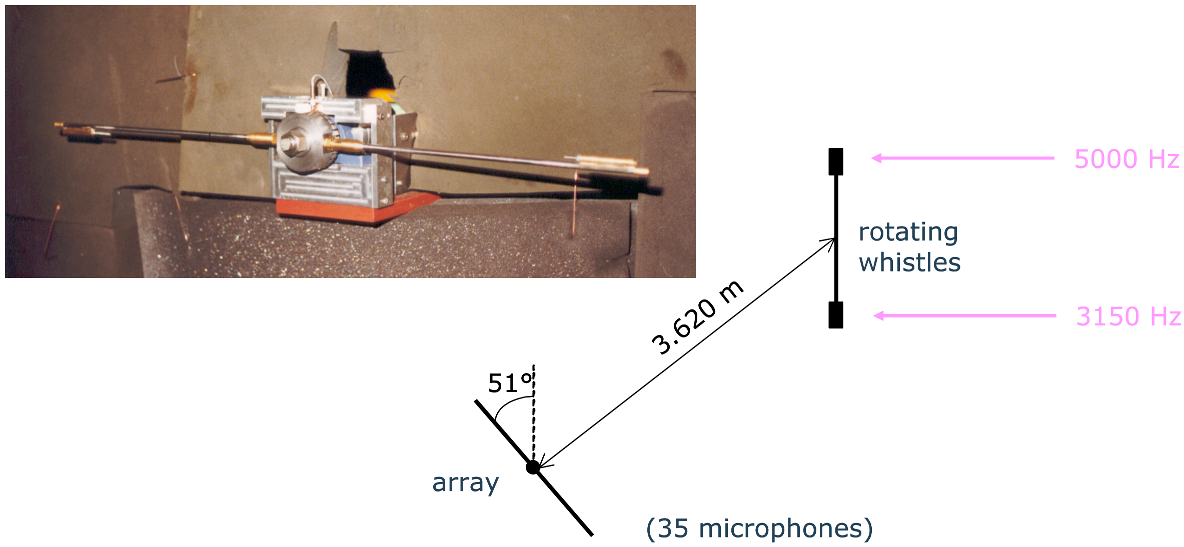

Fig. 1: Set-up with rotating whistles

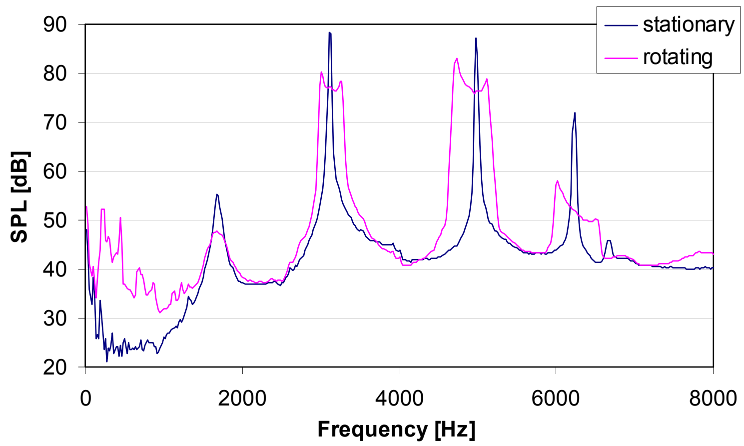

Fig. 2: Average microphone spectra due to whistles

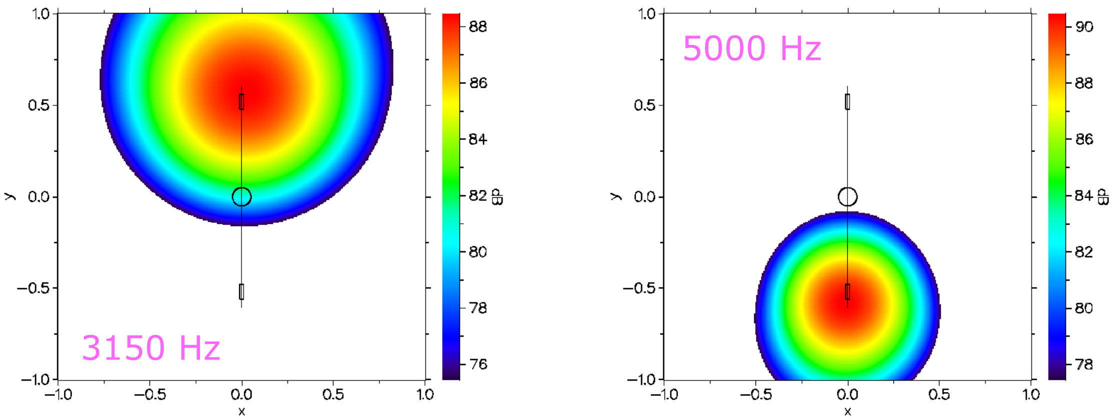

Fig. 3: Results of ROSI beamforming on rotating whistles (plotted on reference geometry)

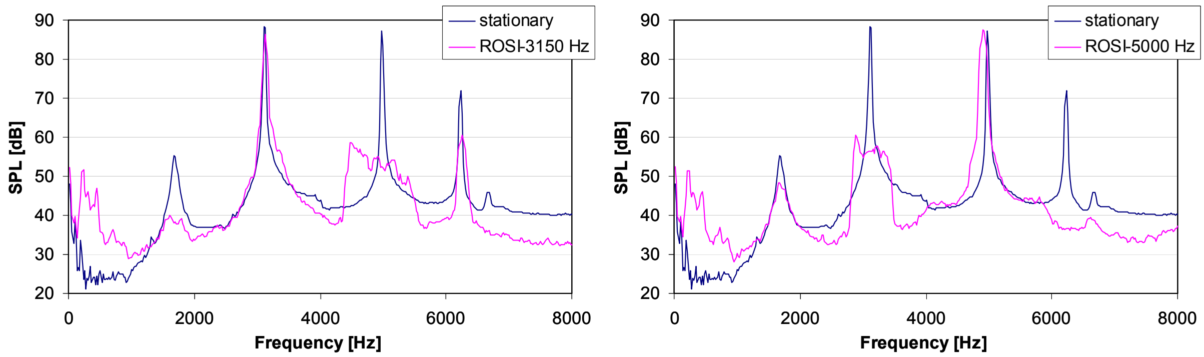

Fig. 4: Whistle spectra obtained with ROSI

3.3 Helicopter blades

In the open configuration of the DNW-LLF, measurements were done on a five-bladed helicopter model with 4 m diameter rotor plane, using a 136 microphone acoustic array (see Fig. 5). To test ROSI, array measurements were used of a "hover" configuration without wind and without shaft angle (horizontal rotor plane). In that case, there is no generation of impulsive blade-vortex interaction noise.

In Fig. 6, typical results (at 2000 Hz, 1/3 octave) are shown. The rotational speed is 852 RPM. The left side shows Conventional Beamforming (CB) results, while the right side shows results of ROSI. The CB results show a circular source region at a short distance from the blade tips. Also, the shadow of the body can be recognized. The ROSI results, however, show clear peaks at the blade positions. In other words, the noise sources are fixed to the blades. The noise mechanism may be (continuous) interaction of the helicopter blades with tip vortices from neighbouring blades.

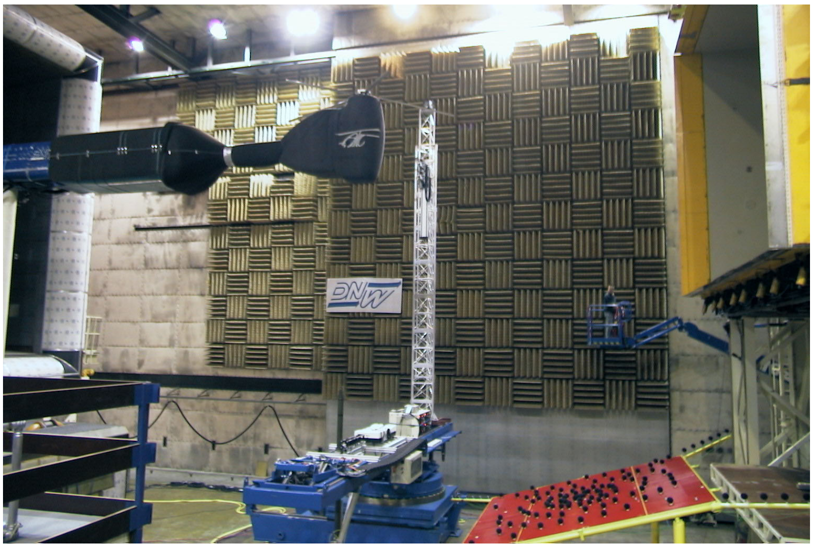

Fig. 5: Set-up with helicopter model and microphone array (shown in red) in DNW-LLF

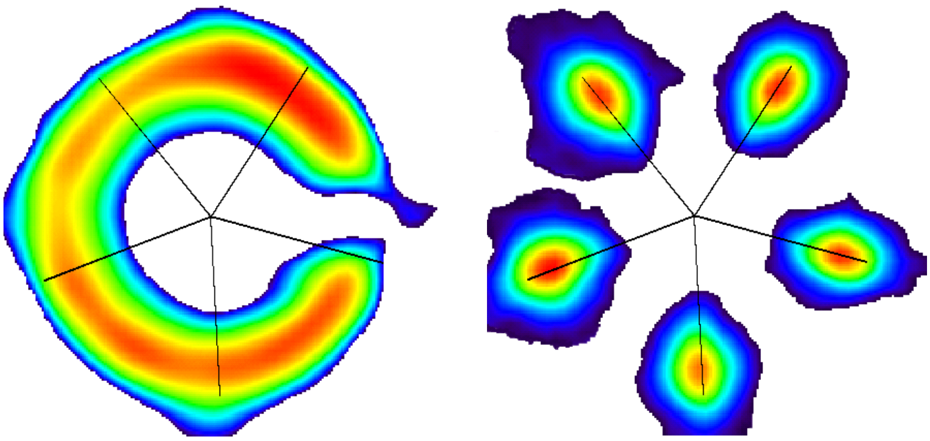

Fig. 6: Noise source maps of helicopter model in hover, obtained with CB (left) and ROSI (right)

3.4 Wind turbine blades

Measurements were done in the open jet of the DNW-LLF on a 4.5 m diameter two-bladed wind turbine rotor model, with the same acoustic array of 136 microphones as used for the helicopter measurements (see Fig. 7). The purpose of the experiments was to determine aerodynamic noise levels of different blades for various conditions (Ref. 8). For the results shown here, the RPM was 424, the tunnel speed was 14 m/s, and the yaw angle was 0°.

In Fig. 8, typical noise source maps are shown, obtained with CB and ROSI. Note that the CB results show that most noise is coming from the downward moving part of the rotor. This can be explained by a combination of source directivity and convective amplification (Ref. 16). This asymmetry is averaged out by ROSI, because beamforming is done during full rotations of the rotor blades.

Again, ROSI clearly shows its values. At one of the blades, close to the hub, ROSI shows a remarkable sound source at the leading edge. The location of this source was found to be the junction of two different blade shapes. To further illustrate the capabilities of ROSI, Fig. 9 shows the effect of trailing edge treatment (“serrations”). For the same rotor and identical conditions, a clear reduction is observed in trailing edge noise levels at the location of the serrations.

Fig. 7: Set-up with wind turbine model in DNW-LLF

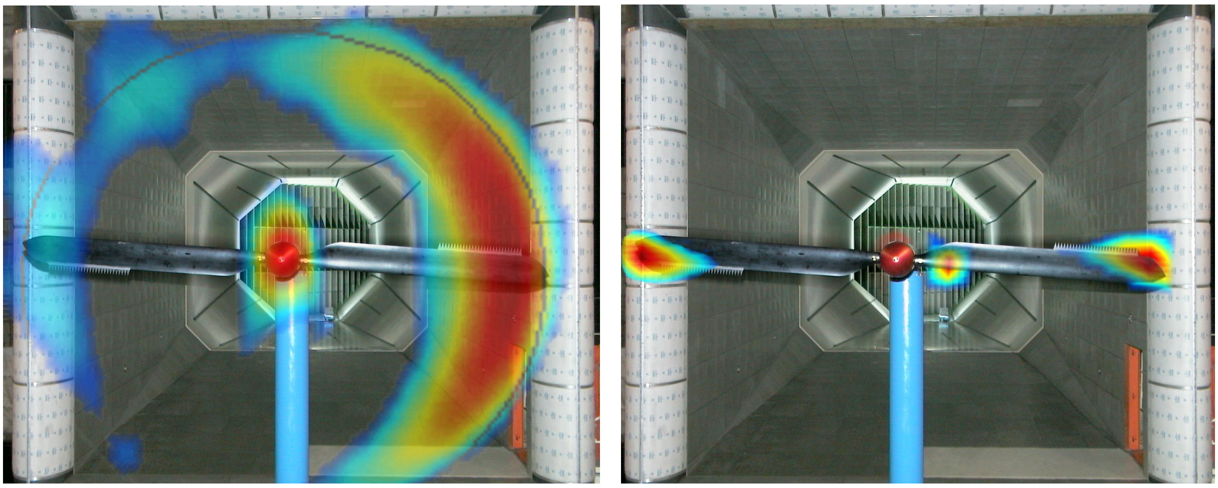

Fig. 8: Noise source maps of wind turbine model, obtained with CB (left) and ROSI (right)

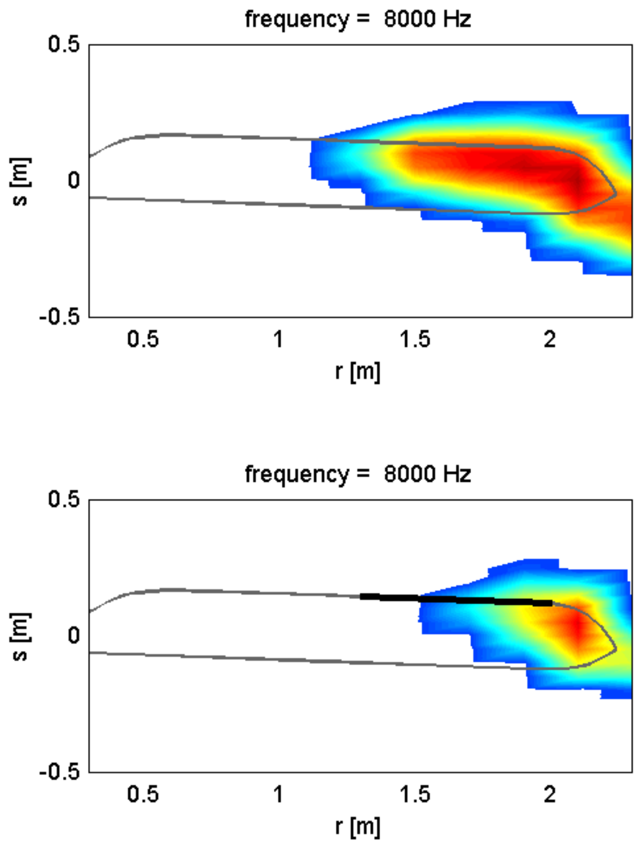

Fig. 9: Effect of trailing edge serrations on radiated trailing edge noise, for the same rotor and identical flow conditions; the lower plot shows the results with serrations

4 Fly-over measurements

Aircraft fly-over array measurements can be used to investigate the noise of individual airframe noise components and to assess the model scale effects of wind tunnel measurements (Ref. 17). Moreover, fly-over array measurements can be valuable for making a breakdown of all possible noise sources, including engine noise, so that their relative contributions to the total noise perceived on the ground is known (Ref. 10).

4.1 Test campaign at Schiphol Airport

In September 2002, NLR performed microphone array measurements on landing aircraft at Amsterdam Airport Schiphol (see Fig. 10). During three days of measurements, 484 fly-over events were recorded. The average fly-over altitude above the array was 43 m; the average speed was 68 m/s. Many aircraft types were included. Most fly-over events were recorded with an array of 243 microphones, which were located within a circle of 6 m radius. This array was located at a distance of about 750 m from the threshold of the “Kaagbaan” runway.

To process the measured array data using the theory of Chapter 2, the computer program MOSI was written. The basis of this program is the same as for ROSI, except that the rotating motion is now replaced by a steady, linear motion.

The measurements provided an extensive data set of aircraft noise sources. Moreover, also information on the array measurement technique itself was obtained, including possibilities for future improvements. One of the new methods that were developed afterwards was a technique, based on source power integration, to determine absolute contributions of aircraft noise components (Ref. 10).

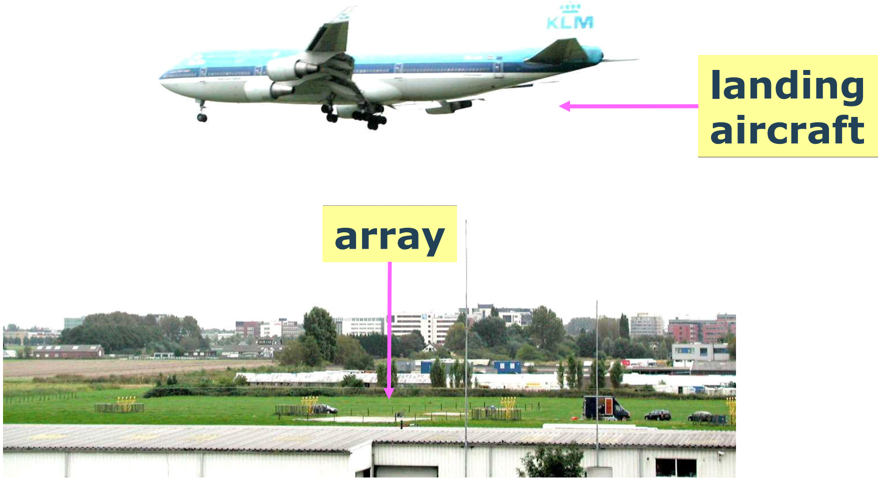

Fig. 10: Array measurements at Schiphol Airport

4.2 Aircraft tracking

Because of the large number of fly-over events at Schiphol, it was desired to have available a system that determines aircraft speed and altitude automatically, i.e., without the cumbersome manual processing that is needed with video cameras or laser systems. Therefore, a tracking system was developed using 5 passive light sensors mounted in tubes, 3 of which are pointing vertically (90º), and two of which point at 45º (Fig. 11). The AC-components of the sensor output signals were recorded simultaneously with the microphones.

The signals from the different sensors were well correlated, as can be seen in the example of Fig. 12. Therefore the time difference between the sensor signals, in other words, the differences in time that the airplane passes the beams, can be calculated automatically. This was done by a cross-correlation analysis, viz. by searching the maximum values of the cross-correlation functions. The ground speed was determined using the signals of the three 90º sensors, the altitude was determined on two locations using the additional information from the 45º sensors.

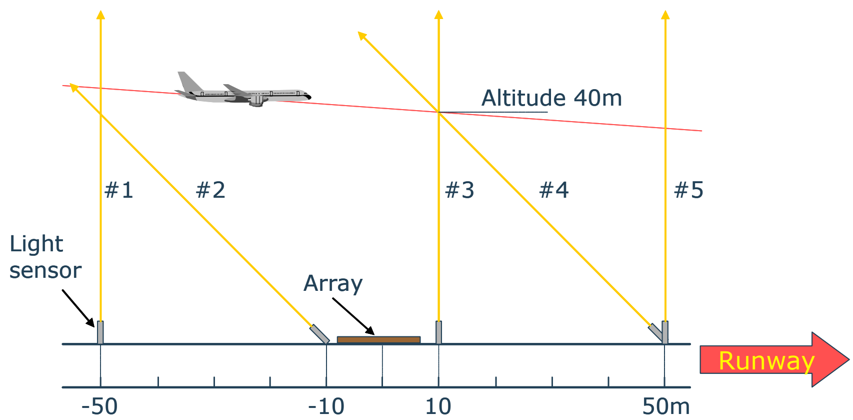

Fig. 11: Positions and orientations of the light sensors

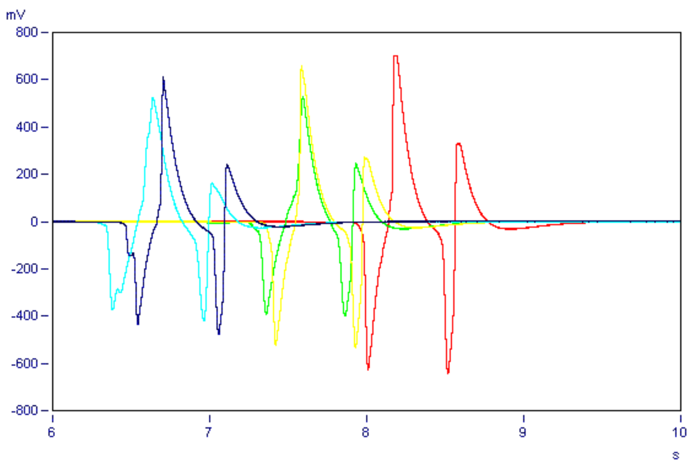

Fig. 12: Signals from light sensors from a single fly-over event

4.3 Array design

The array was designed to have good performance in the frequency range 500 – 6000 Hz. In this range the array is required to low side lobe levels and high resolution (narrow beam widths). The maximum radius for the microphone array was 6 m. The number of data channels available for microphones was 243.

In a previous measurement campaign at Schiphol Airport (September 2000) it was found that the array resolution is limited by loss of coherence due to atmospheric turbulence (Refs. 18-20). During propagation from noise sources on the aircraft to microphones on the ground, the sound signals are distorted by turbulence. This distortion is different from microphone to microphone, which results in loss of coherence between the different microphone signals. Loss of coherence progressively depends on distance between microphones, and on frequency. For high frequencies, the outer microphones of the array are completely incoherent with the other microphones, and thus the effective aperture of the array is smaller than its physical size.

Quantifying the coherence loss is difficult. In the literature, there is no description of coherence loss of sound that propagates in vertical direction through the atmosphere. Also, it can not be deduced immediately from the fly-over measurements. Loss of coherence can be perceived indirectly from the fly-over measurements. This can be done by processing array data of a single fly-over event with different array sizes (Ref. 21), and comparing the resultant noise source maps. First, an array processing can be done with the entire array, and then the outer part of the array can be excluded from the processing. If the outer microphones are affected by loss of coherence, they do not contribute effectively to the beamforming process, but they only add noise. Then, reduction of array size will *not* result into lower resolution. Instead, the peak levels will increase and the noise levels in the source maps will decrease.

By performing such a study with different array sizes, using data from the previous Schiphol measurement campaign, it was found that the radius of the effective array aperture is approximately

$$R = 4000/f \; . \tag{31}$$

In other words, the effective array aperture at 4000 Hz is approximately a disk of 1 m radius. At other frequencies the effective array aperture is inverse proportional to the frequency.

In order to have high array performance at the entire frequency range of interest, it is required to have available a sufficiently large number of microphones for each frequency. This holds in particular for the highest frequencies, where the effective array aperture (31) is small. Therefore, an array design was made with a high microphone density in the central part of the array, and more sparsely spaced microphones in the periphery (see Fig. 13). The effects of frequency-dependent effective array apertures were incorporated in the beamforming process, by applying a frequency-dependent spatial window (Refs. 9, 10).

A drawback of an array design with densely spaced microphones in the central part, and more sparsely spaced microphones in the outer part, is that the array resolution is not optimal. If all microphones are processed with the same weight, then too much emphasis is put on the central part. Consequently, the array resolution is less than the resolution of a continuous disk (or elliptic mirror) of the same size.

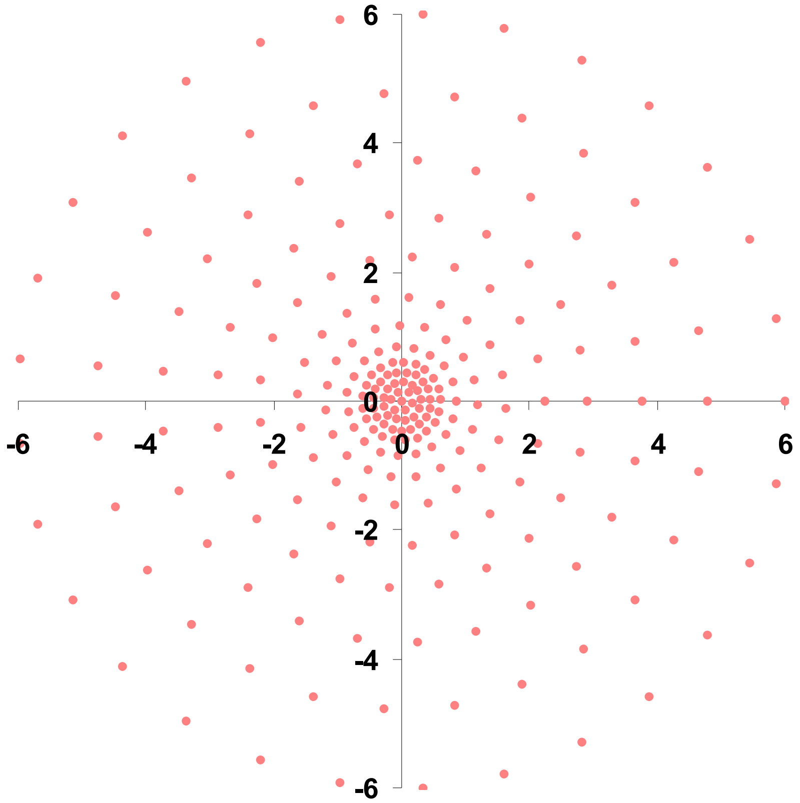

Fig. 13: Microphone layout for Schiphol fly-over measurements

This drawback is countered by weighting the microphone signals in the beamforming process (Refs. 9, 10). These weights are proportional to the area surrounding each microphone, so that the processed acoustic power per unit area is approximately constant. With the array shown in Fig. 13 this microphone-dependent area association is indeed possible. The array is built up by a number of concentric rings with increasing spacing towards the outer part. The spacing between rings is kept, as much as possible, the same as the spacing between two adjacent microphones in a ring. Thus, an area association is straightforward.

4.4 Typical results

Typical MOSI results are shown in Fig. 14 for an MD82 aircraft, and in Fig. 15 for some other aircraft types.

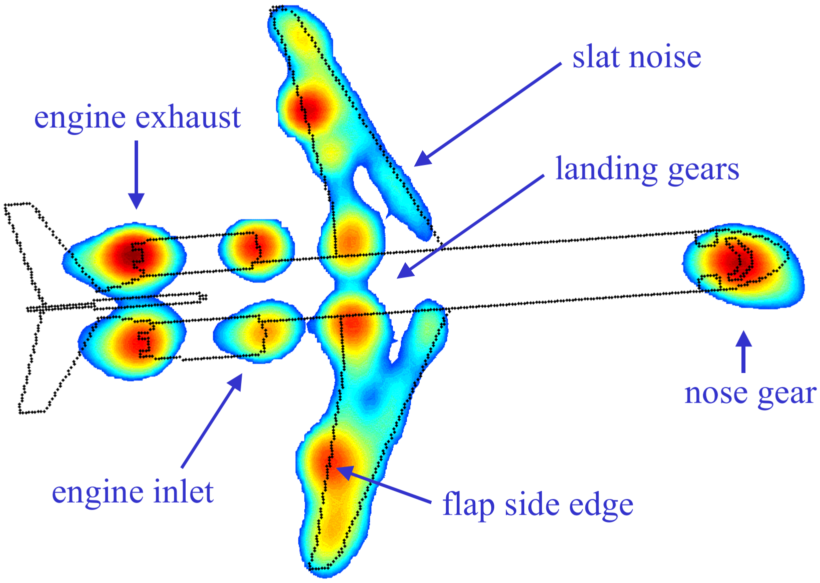

Fig. 14: Noise source map of an MD82 aircraft; 1600 Hz 1/3 octave band

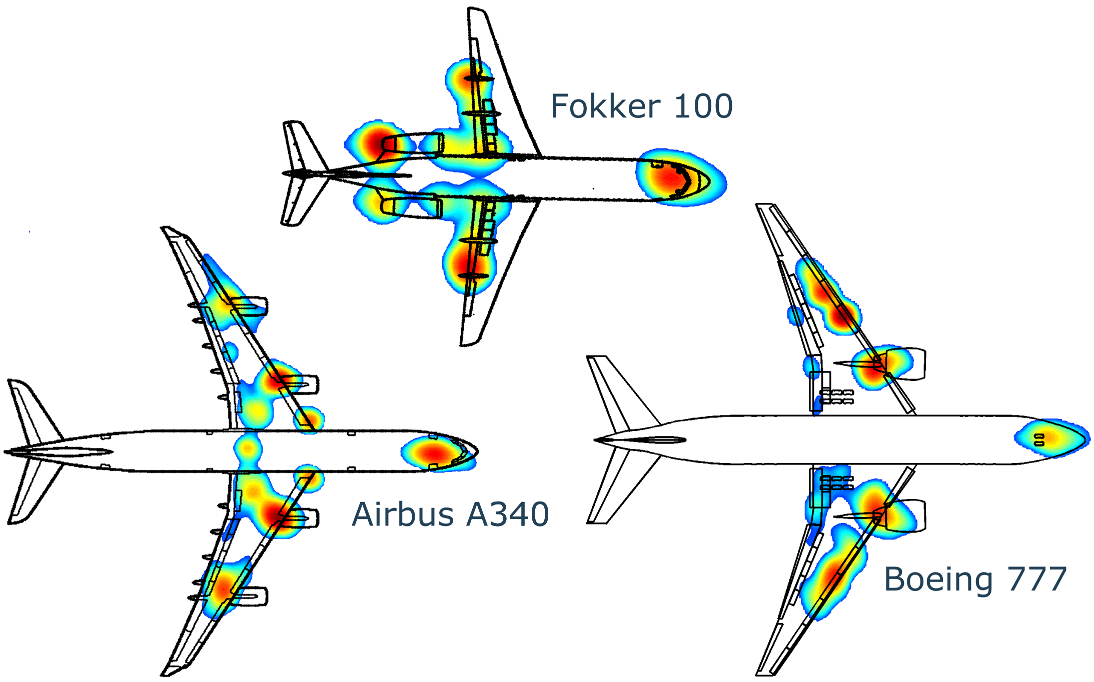

Fig. 15: Typical noise source maps of other aircraft types

References

1. Takano, Y., Horihata, K., Kaneko, R., Matsui, Y., and Fujita, H., Analysis of sound source characteristics of Shinkansen cars by means of x-shaped microphone array, Internoise 96, Liverpool, 1996.
2. Barsikow, B., Experiences with various configurations of microphone arrays used to locate sound sources on railway trains operated by the DB AG, *Journal of Sound and Vibration*, Vol. 193, No. 1, pp. 283-293, 1996.
3. Michel, U., Barsikow, B., Helbig, J., Hellmig, M., and Schüttpelz, M., Flyover noise measurements on landing aircraft with a microphone array, AIAA Paper 98-2336, 1998.
4. Piet, J.-F., and Elias, G., Localization of acoustic source from a landing aircraft with a microphone array, AIAA Paper 99-1811, 1999.
5. Barsikow, B., and King III, W.F., On removing the Doppler frequency shift from array measurements of railway noise, *Journal of Sound and Vibration*, Vol. 120, No. 1, pp. 190-196, 1988.
6. Howell, G.P., Bradley, A.J., McCormick, M.A., and Brown, J.D., De-Dopplerization and acoustic imaging of aircraft fly-over noise measurements, *Journal of Sound and Vibration*, Vol. 105, No. 1, pp. 151-167, 1986.
7. Sijtsma, P., Oerlemans, S., and Holthusen, H.H., Location of rotating sources by phased array measurements, AIAA Paper 2001-2167, 2001.
8. Oerlemans, S., Schepers, G., Guidati, G., and Wagner, S., Experimental demonstration of wind turbine noise reduction through optimized airfoil shape and trailing-edge serrations, presented at the European Wind Energy Conference and Exhibition, Copenhagen, Denmark, 2-6 July 2001.
9. Sijtsma, P., and Wal, H.M.M. van der, Identification of noise sources on civil aircraft in approach using a phased array of microphones, NATO-RTO-MP-SET-079-24, presented at the NATO RTO SET Symposium on “Capabilities of Acoustics in Air-Ground and Maritime Reconnaissance, Target Classification and –Identification”, Lerici, Italy, 26-28 April 2004.
10. Sijtsma, P., and Stoker, R.W., Determination of absolute contributions of aircraft noise components using fly-over array measurements, AIAA Paper 2004-2958, 2004.
11. Howe, M.S., *Acoustics of Fluid-Structure Interactions*, Cambridge University Press, 1998.
12. Dowling, A.P., and Ffowcs Williams, J.E., *Sound and Sources of Sound*, Wiley, 1983.
13. Treves, F., *Basic Partial Differential Equations*, Academic Press, 1975.
14. Amiet, R.K., Refraction of sound by a shear layer, *Journal of Sound and Vibration*, Vol. 8, No. 2, pp. 467-482, 1978.
15. Schulten, J.B.H.M., Computation of Aircraft Noise Propagation through the Atmospheric Boundary Layer, Proc. 5th Int. Congress on Sound and Vibration, Adelaide, Australia, 1997.

16. Oerlemans, S., Sijtsma, P., and Méndez López, B., Location and quantification of noise sources on a wind turbine, *Journal of Sound and Vibration*, to be published, available online 4 October 2006.
17. Stoker, R.W., Guo, Y., Streett, C., and Burnside, N., Airframe noise source locations of a 777 aircraft in flight and comparisons with past model-scale tests, AIAA Paper 2003-3232, 2003.
18. Tatarski, V.I., The effects of the turbulent atmosphere on wave propagation, Israel Program for Scientific Translations, Jerusalem, 1971.
19. Tatarski, V.I., *Wave Propagation in a Turbulent Medium*, McGraw-Hill, 1961.
20. Dougherty, R.P., Turbulent decorrelation of aeroacoustic phased arrays: Lessons from atmospheric science and astronomy, AIAA Paper 2003-3200, 2003.
21. Brooks, T.F., Humphreys Jr., W.M., Effect of directional array size on the measurement of airframe noise components, AIAA Paper 99-1958, 1999.